PCCP

PAPER

View Article Online
View Journal

Cite this: DOI: 10.1039/c6cp00887a

Thermophysical properties of $LiCoO_2$–$LiMn_2O_4$ blended electrode materials for Li-ion batteries

Petronela Gotcu* and Hans J. Seifert

Thermophysical properties of two cathode types for lithium-ion batteries were measured by dependence on temperature. The cathode materials are commercial composite thick films containing $LiCoO_2$ and $LiMn_2O_4$ blended active materials, mixed with additives (binder and carbon black) deposited on aluminium current collector foils. The thermal diffusivities of the cathode samples were measured by laser flash analysis up to 673 K. The specific heat data was determined based on measured composite specific heat, aluminium specific heat data and their corresponding measured mass fractions. The composite specific heat data was measured using two differential scanning calorimeters over the temperature range from 298 to 573 K. For a comprehensive understanding of the blended composite thermal behaviour, measurements of the heat capacity of an additional $LiMn_2O_4$ sample were performed, and are the first experimental data up to 700 K. Thermal conductivity of each cathode type and their corresponding blended composite layers were estimated from the measured thermal diffusivity, the specific heat capacity and the estimated density based on metallographic methods and structural investigations. Such data are highly relevant for simulation studies of thermal management and thermal runaway in lithium-ion batteries, in which the bulk properties are assumed, as a common approach, to be temperature independent.

Received 8th February 2016,
Accepted 13th March 2016

DOI: 10.1039/c6cp00887a

www.rsc.org/pccp

Introduction

During recent years, the strong demand of batteries with excellent performance has increased the interest in the research and development of lithium-ion batteries, with the highest energy density among rechargeable batteries. Significant efforts were dedicated to improve the cathode materials. One approach refers to blended cathodes for which the active material is a physical mixture of two (or more) distinct lithium intercalation compounds.[1] The new chemistries focus on well-known and already in use materials[2,3] such as lithium cobalt oxide, $LiCoO_2$, with a layered structure, and the spinel lithium manganese oxide, $LiMn_2O_4$, in order to achieve a more balanced performance in comparison to that of the individual component. In this way, the main drawbacks of $LiCoO_2$ cathodes, the high costs, the limited practical capacity due to structural and chemical instabilities at deep charge ($x < 0.5$ in Li_xCoO_2), and the susceptibility to thermal runaway, are compensated by the addition of $LiMn_2O_4$, with lower costs and sufficiently high charge voltage.[4] Furthermore, the fading of the capacity of cathodes containing $LiMn_2O_4$ during cycling, due to the dissolution of Mn-ion in the electrolyte and the migration to the negative electrode, was decreased by using instead a mixture of $LiMn_2O_4$ and layered cathode materials.[3] In addition, a more balanced performance was achieved and the thermal stability of these cathode materials was increased in comparison to that of the individual component. In an attempt to improve the battery safety, thermal management systems (TMS) were introduced for the control of high power and energy density batteries. Thus, thermophysical properties such as thermal conductivity, heat capacity and thermal diffusivity are required for the development of prediction models of the batteries thermal behaviour and a well optimisation of the TMS.

This paper reports the thermophysical properties by dependence with temperature of the cathode materials typically used in lithium-ion batteries production. The cathode materials under investigation are commercial composite thick films containing an active material mixed with additives (binder and carbon) deposited on aluminium current collector foils. All the samples used in this study are dry materials, as purchased from the manufacturer. Since most of the cell and battery pack models consider a homogeneously distributed mixture of liquid electrolyte in the porous electrodes, the data provided in this study could contribute to the improvement of such models by implementation of dry areas which coexist within cell layers.[5] These areas represent sources of ageing and degradation and lead to thermal gradients across the cells, which are generally neglected in state of the art TMS.

Institute for Applied Materials – Applied Materials Physics (IAM-AWP), Karlsruhe Institute of Technology, Germany. E-mail: petronela.gotcu-freis@kit.edu, hans.seifert@kit.edu

The thermophysical properties of the composite layers, with two different active material composition, blends of $LiCoO_2$ and $LiMn_2O_4$, were studied as a function of temperature up to 673 K. Thermal conductivity data were determined from thermal diffusivity measured by laser flash analysis, specific heat capacity measurements by calorimetric methods and density estimations. Furthermore, in order to understand the complex behaviour of the composite samples, estimations were made from the heat capacities of the constituent compounds. In this purpose, heat capacity measurements were performed on a pure $LiMn_2O_4$ additional sample, representing the first experimental $LiMn_2O_4$ heat capacity data up to 700 K. Together with the heat capacity data already obtained in our lab on $LiCoO_2$,[6] these results confirmed the independently measured thermal behaviour of the blended composites.

The results presented in this work are the first experimental data which combine application oriented and fundamental research. Such data are highly relevant for simulation studies of thermal behaviour including thermal runaway of lithium-ion batteries, in which the bulk properties are assumed, as a common approach, to be temperature independent.

Samples and their characterisations

The lithium-ion battery cathode materials used in this study were purchased from MTI Corporation, USA[7] and stored in a glove box (water and oxygen levels, each below 0.1 ppm) under an argon (mass fraction purity 99.9999) atmosphere. The commercial cathode materials are based on current collector layer represented by the aluminium foil (substrate) coated on a single side by a composite layer, which is a mixture of active materials and additives. Such cathode materials are produced by a tape cast process, followed by calendaring, during which the particle–particle contact and the composite adhesion to the current collector are substantially improved. Two cathode types were considered in this study, containing active materials with different composition blends of both $LiCoO_2$ and $LiMn_2O_4$. The supplier's information on the mass fraction of the active material in powder was 0.950 for the $LiCoO_2$ rich cathode and 0.945 for the $LiMn_2O_4$ rich cathode, whereas the specific capacities of the cathodes were 145 mA h g^{-1} and 110 mA h g^{-1}, respectively. These electrodes provide similar current density ($\sim$3 mA cm^{-2}) for charging/discharging in 1 h. The included additives are carbon and polyvinylidene fluoride (PVDF) binder, for which the exact amount was not provided. In addition to the cathode materials, an $LiMn_2O_4$ powder sample with a general formula $Li_{1+x}Mn_{2-x}O_4$, with x in the range of 0.00–0.02, purchased from the same supplier,[7] was used in this study.

The layers of each sample were as well individually investigated. For this purpose, the composite layer was mechanically removed from the aluminium foil. The main components in the blended composite layer were identified by inductively coupled plasma optical emission spectrometry analysis (ICP-OES, OPTIMA 4300 DV from Perkin Elmer). The carbon content was determined with a CS600 Analyser from Leco Corporation, USA. Aluminium foil, which plays the role of current collector in the cathode sample, was investigated using wavelength dispersive X-ray fluorescence analysis (WDXRF) with a S4 PIONEER, Bruker-AXS.

Room temperature X-ray diffraction was performed directly on the cathodes (composite side) in a D4 Endeavor diffractometer (Bruker-AXS GmbH, Karlsruhe, Germany) using Cu Kα radiation with an excitation of 40 kV at 40 mA. The diffraction patterns were recorded in the angle range of $0^\circ < 2\theta < 162^\circ$ with a step size increment of 0.02° and a collection time of 7 s per step. The phase fractions and the lattice parameters were determined using Rietveld refinement analysis software TOPAS 4.2 (Bruker, Germany).

Metallographic methods such as light microscopy (LM) and scanning electron microscopy (SEM) were used for structural investigations, prior and post thermophysical measurements. Since a major source of error in the calculation of the thermal diffusivity is related to the thickness of the sample, this had to be accurately measured. The cathodes were also investigated using LM cross section analysis. The samples were embedded under vacuum in a resin material mixed with fluorescent additive, followed by grinding and polishing. The image processing software (ProgRes® CapturePro from Jenoptik/Optical Systems, Germany) and the image analysis software (AnalySis docu from Olympus Soft Imaging Solutions GmbH, Germany) enabled evaluation of the thickness of each constituent layer. A total of 20 measurement points on a sample were considered, with one measurement at each 100 μm. Phase analysis was also applied and the porosity content was estimated using the same software. Additionally, the mercury intrusion porosimetry technique was employed for the $LiCoO_2$ rich cathode to measure the total pore volume in our samples. Two instruments were used, a Pascal 140 for the measurements of the macropores (>50 nm) and a Pascal 440 for the measurements of the mesopores (2–50 nm), both from Porotec GmbH, Germany.

Thermophysical investigations

Prior to all measurements, the samples were annealed at 400 K for 12 h in an oven under vacuum in order to ensure water-free samples.

The specific heat capacity data c_p of the cathodes were determined from the specific heat of the constituent components (substrate and composite layers) and their corresponding mass fraction contributions. Specific heat measurements on the composite blends were performed using two differential scanning calorimeters. Continuous method was applied on a DSC 204 F1 Phoenix® (DSC 204) between 298 and 523 K and a DSC 404 F1 Pegasus® (DSC 404) between 455 and 573 K, respectively (both instruments from Netzsch GmbH, Selb, Germany). Since compact samples were required for these measurements, disks of 5 mm diameter and a weight of 40–45 mg were prepared from the powder composite material removed from the aluminium current collector. The measurements were carried out in argon gas flow (mass fraction purity 0.99999). The experimental

procedure and data evaluation are described elsewhere,[6] to which we refer for more details.

In order to understand the thermal behaviour of the blended composite samples, their specific heat data were also estimated from the specific heat capacity data of their constituent compounds and their respective mass fraction. Thus, the specific heat of the supplementary $LiMn_2O_4$ sample was measured in our lab using the same procedure as for the blended composites in the temperature range from 298 to 700 K.

The thermal diffusivity of the cathode materials was measured using a laser flash analyser LFA-1000 from Linseis GmbH, Germany.[8] All measurements were carried out in He atmosphere (mass fraction purity 0.99999). For each measurement, a minimum of three samples of each type were prepared. Round sample holders made of SiC with a diameter of 12.7 mm were used.

The cathodes are fragile samples and therefore not easy to handle. In order to maintain their quality during preparation, cathodes were cut in the shape of 12.7 mm diameter disks by a Tangerine femtosecond laser from Amplitude Systèmes, France. Such a laser type was used to minimise the thermal impact into the material, to reduce debris formation and avoid melting during the cutting process.[9,10] The parameters used for cutting these materials were: 515 nm wavelength, 350 fs pulse duration, 20 μm focus diameter, 4.6 W average laser power, 200 kHz laser repetition rate, 80 mm s^{-1} laser scan speed, with a total of 6 laser scans for one cut. After this step, the samples were spray coated on the metal side with graphite (Graphit 33, CRC Industries Europe, with relative density 0.84 g cm^{-3}) to ensure a high and a homogeneous absorption of the laser beam in the LFA.

In the LFA-1000 the laser beam, produced by a Nd:YAG laser source, is directed vertically. The energy of the pulse (up to 25 J per pulse) is absorbed on the front surface side of the sample. As a result, the temperature rise on the rear side of the sample is detected by a InSb type sensor (cooled by liquid nitrogen) and measured as a signal voltage as function of time. The analyser is equipped with a carousel sample holder which allows subsequent measurements of six samples. A thermocouple type-S is located at the centre of the carousel holder.

Under adiabatic conditions and for short laser pulses the thermal diffusivity (α) of a sample is directly dependent on the sample thickness and the half-time, defined as the half of the time which is needed to reach the maximum temperature.[11] However, corrections for heat pulse duration and heat loss in the sample were considered and correction models from the Linseis software were applied to our measurements. The combined model[12] was used which includes both heat loss and finite pulse corrections. Furthermore, the thermal diffusivity of the cathode samples was estimated using the three-layer model,[13,14] where each of the sample constituents, the blended composite, aluminium and graphite coating, represent individual layers.

Thermal diffusivity of the samples was initially measured as a function of temperature from 298 K up to 373 K. Furthermore, the temperature was increased up to 473 K, above the melting temperature of the binder, reported to occur in the range of 433–445 K.[7] The samples were annealed at 473 K for 12 h, to ensure the homogeneity of the melting and thereafter were cooled down and measurements were repeated. The same procedure was applied up to the next target temperatures of 573 K and 673 K. Generally, the thermal diffusivity was measured on both heating and cooling ramps to ensure that the measured values refer to respective stable compositions during the total measurement time. The target temperature was achieved with increasing/decreasing rates of 2 K min^{-1} and isothermal segments of at least 0.5 h were introduced at the temperature of interest in order to minimise the dynamics of the system. A minimum of 5 laser shots, with a pulse duration between 0.2 to 0.5 ms and a break time of 1 minute between shots were applied for each sample.

Thermal conductivity data of each cathode type and corresponding blended composite layer were obtained by multiplying the measured thermal diffusivity, specific heat capacity and the estimated density.

Results and discussion

Sample stoichiometry and layers composition

The WDXRF results of the aluminium substrate of both sample types showed a mass fraction of Al larger than 0.99. ICP-OES and XRD analyses indicated a mixture of lithium cobalt and manganese oxides in the composite layers. The sample characterisation data are summarised in Table 1.

The Li/M ratios with M = Co + Mn based on the ICP-OES results were found to be 0.892 ± 0.003 and 0.537 ± 0.008 for both blended composite samples. The total mass fraction of the active material in each composite layer was found to be 0.94, which is close to the supplier information, whereas the analysed mass fraction of carbon was 0.045. The remainder was attributed to the binder. In the case of $LiMn_2O_4$ powder, the analysed Li/Mn ratio was 0.524 ± 0.001.

The lattice parameters of the $LiCoO_2$ phase were determined as a = 0.28156(4) nm, c = 1.4053(4) nm and a = 0.2816(2) nm, c = 1.4048(13) nm, respectively, in the both samples. These parameters are in good agreement with the experimental reported values for the O3-phase $LiCoO_2$ which are in the range of 0.2814 to 0.2817 nm for the a-parameter and 1.405 to 1.408 nm for the c-parameter.[15,16] Furthermore, Rietveld refinement analysis indicated the presence of the $LiMn_2O_4$ phase with a mass fraction below 0.20 and above 0.90, respectively. Our XRD resulting lattice parameters for $LiMn_2O_4$ were a = 0.8234(3) nm and a = 0.8230(1) nm, which according to Gao and Dahn[17] and Wang and Navrotsky,[18] indicate a $Li_{1+x}Mn_{2-x}O_4$ stoichiometry corresponding to x between 0.025 and 0.035. Assuming that the active material composition in the cathode is a mixture of $LiCoO_2$ and $Li_{1+x}Mn_{2-x}O_4$, from the ICP-OES results we obtain a composition corresponding to $1 + x = 1.030 \pm 0.005$, in agreement with the XRD data. The lattice parameter of the $LiMn_2O_4$ phase in the powder sample was found to be a = 0.82294(18) nm, similar to that of the composite blends. The obtained stoichiometry from the measured lithium and manganese ion concentrations by following the supplier data

Table 1 Description of the sample components, mass fraction purity and the analysis method for purity determination of the lithium-ion battery cathode based on aluminium foil coated on a single side by an $LiCoO_2$–$LiMn_2O_4$ blended composite layer

Sample and sample components		Chemical name	Mass fraction purity	Analysis method
$LiCoO_2$ rich sample	Composite layer	$LiCoO_2$	0.75	ICP-OES
			0.80	XRD
		$LiMn_2O_4$	0.19	ICP-OES
			0.18	XRD
		$LiCoO_2$ + $LiMn_2O_4$ (active material mixture)	0.94 (0.950)[a]	ICP-OES
			0.98	XRD
		C	0.045	CS analyser
			0.02	XRD
	Aluminium foil	Al	0.99[b]	WDXRF
$LiMn_2O_4$ rich sample	Composite layer	$LiMn_2O_4$	0.91	ICP-OES
			0.90	XRD
		$LiCoO_2$	0.03	ICP-OES
			0.02	XRD
		$LiCoO_2$ + $LiMn_2O_4$ (active material mixture)	0.94 (0.945)[a]	ICP-OES
			0.98	XRD
		C	0.045	CS analyser
			0.08	XRD
$LiMn_2O_4$ powder sample		$LiMn_2O_4$	0.999 (>0.98)[a]	ICP-OES
			0.99	XRD

[a] The number within the brackets represents the initial mass fraction purity as given by the supplier. [b] The WDXRF analyses show the same results for aluminium foils in the both cathode samples.

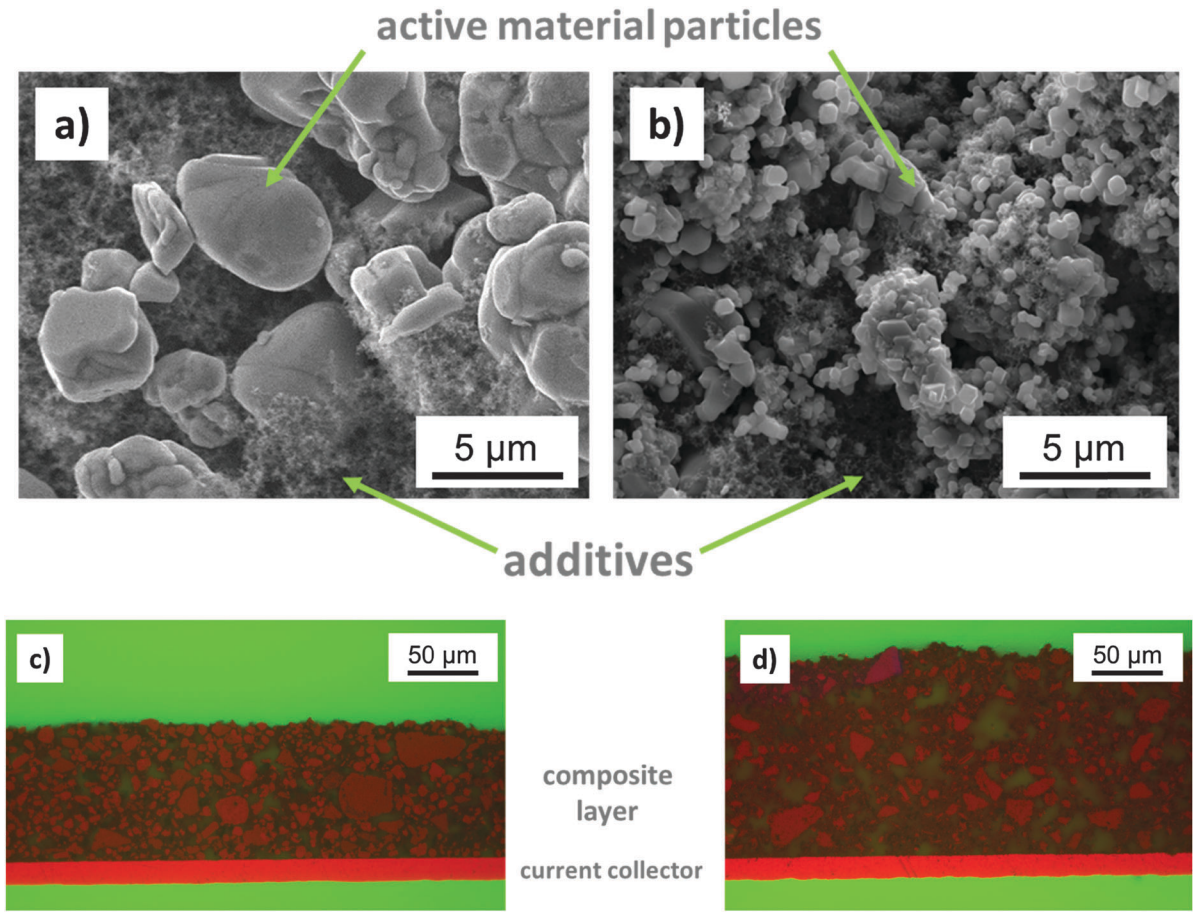

Fig. 1 Lithium-ion battery cathode samples based on aluminium foil coated on a single side by $LiCoO_2$–$LiMn_2O_4$ blended composite layer. (a and c) represent an $LiCoO_2$ rich sample, whereas (b and d) represent an $LiMn_2O_4$ rich sample. (a and b) are the SEM images (top view), whereas (c and d) are the LM images (cross section view). In the LM images it can be observed that within the composite layer the pores are filled with the resin material mixed with the fluorescent additive (green) which embeds the whole of the sample.

sheet when the Li/Mn molar ratio equals $(1 + x)/(2 - x)$ was $x = 0.031$ in $Li_{1+x}Mn_{2-x}O_4$, which also confirms the XRD value. The estimated $LiCoO_2 : Li_{1.03}Mn_{1.97}O_{4.00}$ ratio is 3.9 : 1.0 and $Li_{1.03}Mn_{1.97}O_{4.00} : LiCoO_2$ ratio is 29.7 : 1.0, both in good agreement to the mass fractions given by XRD analysis.

With this latter consideration, we further refer to the two $LiCoO_2$–$LiMn_2O_4$ blended cathode types as the $LiCoO_2$-rich cathode sample containing an $LiCoO_2$-rich composite layer and an $LiMn_2O_4$-rich cathode sample containing an $LiMn_2O_4$-rich composite layer, respectively.

The comparison between the two independent results from XRD–Rietveld refinement and ICP-OES analyses leads to a good agreement and confirms the reliability of the obtained data.

Structure and morphology

Fig. 1 shows the top view and the cross section view of both cathode blended materials, (a) and (c) for the $LiCoO_2$ rich sample, (b) and (d) for the $LiMn_2O_4$ rich sample, respectively. The (a) and (b) SEM images clearly show the active material particles having different sizes and shapes. The particles within the $LiCoO_2$ rich sample have a spherical shape and an average size of 6 ± 2 μm, whereas the $LiMn_2O_4$ rich sample consists of a mixture of active material primary particles in shape of cubes with an average size of 0.5 μm and much larger particles up to 15 ± 7 μm. Among the active material, the additives can also be observed. The LM cross section images (c and d) show the aluminium current collector and the composite layer on top of it. The thickness of the aluminium foil was determined as 15 μm (Table 2) in both samples. Alternatively, the foil thickness was estimated based on its weight (weighing accuracy ±0.005 mg) and density taken as 2.7 g cm^{-3},[19] considering the negligible porosity. The results indicated 15 μm, which is consistent with the LM measurements and the supplier data. The thickness of the composite layer analysed by LM in the $LiCoO_2$ rich sample was 95 μm. A higher thickness of 145 μm was found for the composite layer of the $LiMn_2O_4$ rich sample.

Using the measured blended composite layer thickness and the weight of the disk samples, the densities were estimated to be 2.29 ± 0.03 and 1.63 ± 0.03 g cm^{-3}, for $LiCoO_2$ and $LiMn_2O_4$ rich composites, respectively. Furthermore, the corresponding cathodes densities were evaluated and the determined values were 2.34 ± 0.03 and 1.73 ± 0.03 g cm^{-3} (Table 2(a)).

The effective thickness of the graphite spray coating in the disk samples used in the thermal diffusivity measurements was estimated from the weight increase of the samples after coating, yielding graphite layer thicknesses of 5 and 6 μm, respectively.

The porosity was calculated according to ref. 20 taking into account the weight of each sample, the constituent components ($LiCoO_2$, $LiMn_2O_4$, carbon, PVDF) and their densities from ref. 21 for the active materials and from ref. 7 for the additives (Table 2(b)). The resulted porosity values are in good agreement with the mercury porosimetry and the phase analysis data (Table 2(a)).

Furthermore, the current collector to composite mass ratios were determined as 1 : 0.184 and 1 : 0.168 for the $LiCoO_2$ rich and $LiMn_2O_4$ rich cathodes, respectively, based on the total weight of the samples and the weights of the constituent layers (current collector, composite).

Table 2 (a) The properties of the cathode samples and methods of their determination: thicknesses of each layer (μm), porosity (%) and density (g cm^{-3}) of the composite layers and complete cathode samples. (b) Data required for the porosity estimation of the composite layer

(a)

	Cathode sample type	
Properties	$LiCoO_2$ rich sample	$LiMn_2O_4$ rich sample
Thickness (μm): aluminium substrate, LM	15 ± 0.5[a]	15 ± 0.5[a]
Aluminium substrate, estimated	15 ± 0.3[a]	15 ± 0.3[a]
Composite layer, LM	95 ± 2[a]	145 ± 2[a]
Graphite coating, estimated	5 ± 0.5[a]	6 ± 0.5[a]
Density composite (g m^{-3}) × 10^6, estimated	2.29 ± 0.03[b]	1.63 ± 0.03[b]
Density cathode (g m^{-3}) × 10^6, estimated	2.34 ± 0.03[b]	1.73 ± 0.03[b]
Porosity (%): Hg intrusion porosimetry	49 ± 3[a]	—
LM	50 ± 4[a]	56 ± 5[a]
Estimated	48 ± 2[a]	58 ± 2[a]

(b)

Material	Density, (g m^{-3}) × 10^6
$LiCoO_2$	5.05[c]
$LiMn_2O_4$	4.20[c]
PVDF	1.78[d]
Carbon	1.8[d]

[a] The number following the ± symbol is the standard uncertainty calculated based on all the measurement points on each sample. Aluminium substrate and graphite coating thicknesses were estimated from the weight and the density taken as 2.7 g cm^{-3} (negligible porosity)[19] and the weight increase of the samples after coating (weighing accuracy ±0.005 mg), respectively. [b] The expanded uncertainty U, calculated as $U = k \cdot u_c$, where u_c is the combined standard uncertainty calculated based on the measured composite layer thickness, weight and porosity, and k is the coverage factor, $k = 2$ (0.95 level of confidence). [c] From ref. 20. [d] As provided by MTI Corporation, USA.[7]

Thermophysical properties and discussions

Specific heat capacity

The specific heat capacities of the blended composite layer materials are reported in Fig. 2. Fig. 2(a) presents an overview of the measured data compared to the available literature from 0 to 700 K on the constituent compounds in the composite material, including the active material components and the additives. The phase transition around the temperature range 433–445 K, associated with the melting of the binder, is observed in the both samples (dotted lines). At 298 K, c_p($LiCoO_2$ rich composite) = 0.74 J g^{-1} K^{-1} and c_p($LiMn_2O_4$ rich composite) = 0.81 J g^{-1} K^{-1}. The results obtained from the both DSCs, over the common temperature range from 455 to 523 K, agree well with each other (Fig. 2(b) and (c)). The specific heat data were fitted by the least squares method to a Meier–Kelley type, second order polynomial equation with the formula:

$$c_p/(\mathrm{J\ g^{-1}\ K^{-1}}) = A + B\cdot(T/\mathrm{K}) + C\cdot(T/\mathrm{K})^{-2} \quad (1)$$

The obtained A, B and C coefficients are listed in Table 3(a) for two temperature ranges, from 298 to 423 K and from 455 to 573 K.

The specific heat data of the blended composite samples were also estimated from the specific heat capacity data of their

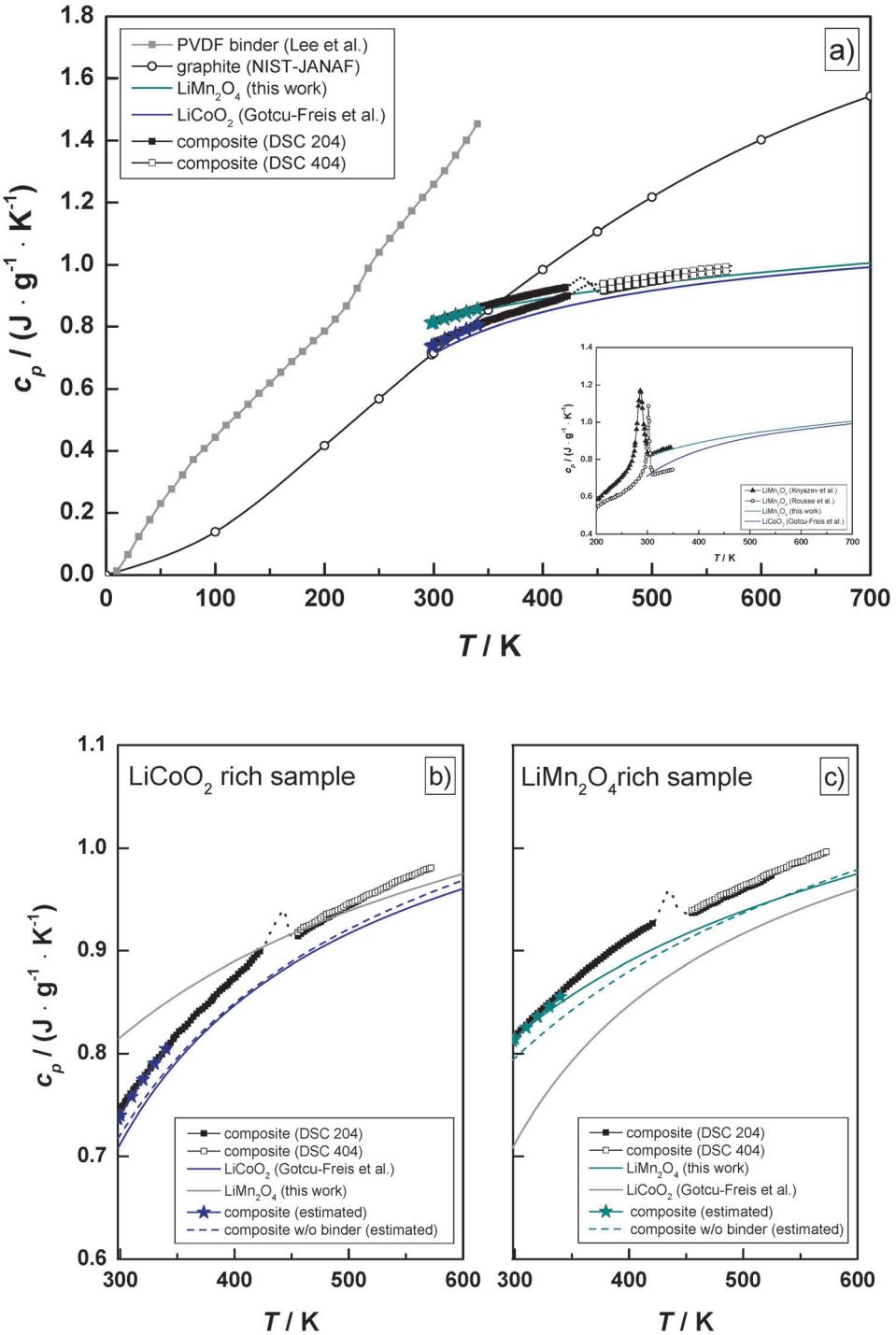

Fig. 2 The specific heat capacity data of the $LiCoO_2$–$LiMn_2O_4$ blended composite layers, part of the cathode materials: (a) data measured in this work and available data on the composite constituent components, (b) measured data on $LiCoO_2$ rich composite and (c) $LiMn_2O_4$ rich composite samples. The uncertainties quoted here are the expanded uncertainties U with $U(c_p)$ = 0.02 J g^{-1} K^{-1} and $U(c_p)$ = 0.01 J g^{-1} K^{-1} for the DSC 204 and DSC 404, respectively, corresponding to a 0.95 level of confidence (k = 2). The blended composite specific heat was estimated from 298 to 340 K from its constituent compounds: PVDF binder specific heat data by Lee *et al.*,[21] carbon data from NIST-JANAF,[23] $LiCoO_2$ values by Gotcu-Freis *et al.*,[6] $LiMn_2O_4$ values from this work, respectively. The dashed lines in (b and c) represent the estimated composite c_p independent of the binder contribution, in the temperature range from 298 to 600 K.

constituent components and their respective mass fraction contributions as given by the sample characterisation described in the previous section and Table 1. For this purpose, the data for the active material components, *i.e.* $LiMn_2O_4$ and $LiCoO_2$, were measured in this work in the temperature range from 298 to 700 K and were taken for $LiCoO_2$ from the recent investigations

Table 3 The polynomial coefficients corresponding to the second order polynomial equation describing the specific heat capacity data, in the temperature ranges from 298 to 423 and from 455 to 573 K, with the formula: $c_p/(J\ g^{-1}\ K^{-1}) = A + B\cdot(T/K) + C\cdot(T/K)^{-2}$ for composite (a) and cathode samples (c), respectively. The specific heat capacity for the $LiMn_2O_4$ sample in the temperature range from 298 to 700 K (b) is described by the following formula: $c_p/(J\ g^{-1}\ K^{-1}) = A + B\cdot(T/K) + C\cdot(T/K)^2 + D\cdot(T/K)^{-0.5} + E\cdot(T/K)^{-2}$

(a)

	$LiCoO_2$ rich composite		$LiMn_2O_4$ rich composite	
Coefficients	298–423 K	455–573 K	298–423 K	455–573 K
A	0.727 ± 0.033	0.963 ± 0.027	0.819 ± 0.008	0.863 ± 0.098
B	$5.889 \times 10^{-4} \pm 6.098 \times 10^{-4}$	$1.658 \times 10^{-4} \pm 3.521 \times 10^{-4}$	$4.089 \times 10^{-4} \pm 1.455 \times 10^{-5}$	$3.004 \times 10^{-4} \pm 2.572 \times 10^{-5}$
C	-14206.143 ± 1445.080	-25232.128 ± 2382.338	-11396.347 ± 329.432	-12991.015 ± 1731.919

(b)

Coefficients	$LiMn_2O_4$ 298–700 K
A	$2.160 \pm 2.278 \times 10^{-12}$
B	$-8.918 \times 10^{-4} \pm 1.795 \times 10^{-15}$
C	$4.794 \times 10^{-7} \pm 7.106 \times 10^{-19}$
D	$-20.559 \pm 3.837 \times 10^{-11}$
E	$6028.926 \pm 3.940 \times 10^{-8}$

(c)

	$LiCoO_2$ rich cathode		$LiMn_2O_4$ rich cathode	
Coefficients	298–423 K	455–573 K	298–423 K	455–573 K
A	$0.758 \pm 2.776 \times 10^{-4}$	$0.937 \pm 5.566 \times 10^{-4}$	$0.834 \pm 2.571 \times 10^{-4}$	$0.853 \pm 5.155 \times 10^{-4}$
B	$5.278 \times 10^{-4} \pm 5.140 \times 10^{-7}$	$2.019 \times 10^{-4} \pm 7.234 \times 10^{-7}$	$3.782 \times 10^{-4} \pm 4.760 \times 10^{-7}$	$3.145 \times 10^{-4} \pm 6.699 \times 10^{-7}$
C	-13187.003 ± 11.644	-21123.881 ± 48.122	-10857.188 ± 10.783	-10949.313 ± 44.563

performed in our lab[6] for a wide temperature range using three differential scanning calorimeters and two different methods, respectively. The measurements were carried out on the DSC 204 between 298 and 700 K and on DSC 404 between 455 and 700 K, the latter in order to validate the results from the former. The two sets of data are in very good agreement over the common temperature range from 455 to 700 K. The specific heat data were fitted over the whole temperature interval (298–700 K) by the least squares method to a Haas–Fisher type polynomial equation with the formula:

$$c_p/(J\ g^{-1}\ K^{-1}) = A + B\cdot(T/K) + C\cdot(T/K)^2 + D\cdot(T/K)^{-0.5} + E\cdot(T/K)^{-2}, \quad (2)$$

where the obtained *A* to *E* coefficients are listed in Table 3(b).

The resulted specific heat at 298 K on our slightly over-stoichiometric $Li_{1+x}Mn_{2-x}O_4$ sample with $x = 0.03$, $c_p(LiMn_2O_4) = 0.81\ J\ g^{-1}\ K^{-1}$ is in good agreement with the recent reported values by Knyazev *et al.*[22] using adiabatic calorimetry measurements up to 347 K on a stoichiometric $LiMn_2O_4$ sample, showing the existence of the reversible orthorhombic–cubic known phase transition below room temperature (Fig. 2(a), inset graph). These results are not consistent with Rousse *et al.*,[23] who also reported specific heat data of $LiMn_2O_4$ up to 350 K using a heat pulse relaxation method, and a slightly different transition temperature. At 298 K, our measured $c_p(LiMn_2O_4)$ is higher than $c_p(LiCoO_2)$, indicating that $LiMn_2O_4$ has a higher ability to store heat.

The c_p of the additives were taken from Lee *et al.*[24] for PVDF binder, where measurements are reported between 80 and 340 K (and reassessed to 0 K in the same study) and from the NIST-JANAF tables[25] for carbon, for a wider temperature range. The estimated c_p of both blended composite materials in the temperature range from 298 to 340 K are in good agreement with our measured c_p data, as can be observed in Fig. 2(b) and (c). The dashed lines represent the estimated c_p blends, independent of the binder contribution. In both composite samples, the difference between the measured composite specific heat data and the estimated data independent of the binder contribution is about 2–2.5%. Considering all the experimental uncertainties, this value, which thus corresponds to the contribution of the binder in the composite material, is consistent with the analysed material composition (Table 1).

The specific heat of the cathodes was determined from the measured composite c_p, aluminium c_p data from NIST-JANAF[25] and mass fractions (Table 1), at 298 K resulting in $c_p(LiCoO_2$ rich cathode$) = 0.77\ J\ g^{-1}\ K^{-1}$ and $c_p(LiMn_2O_4$ rich cathode$) = 0.83\ J\ g^{-1}\ K^{-1}$, respectively. The specific heat data were fitted using the same type of polynomial eqn (1), with the *A*, *B* and *C* coefficients listed in Table 3(c).

Thermal diffusivity and thermal conductivity

The thermal diffusivity (α) of the cathode samples were evaluated using the Linseis software[8] and its included combined model.[12] Fig. 3 presents the results of both samples from 298 K up to 373 K. Measurements were performed on both sides of the cathodes and the results showed that the orientation of the sample side towards the laser beam does not play a role on the measured values. It can be seen that the thermal diffusivity of

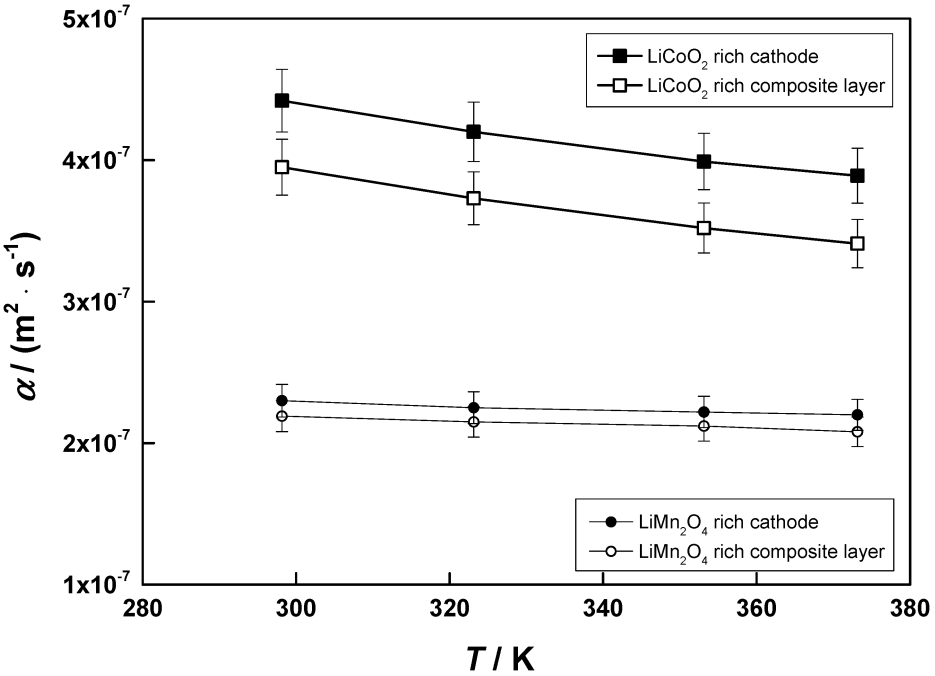

Fig. 3 The thermal diffusivity of the cathode materials (filled symbols) and their corresponding $LiCoO_2$–$LiMn_2O_4$ blended composite layers (empty symbols) as a function of temperature from 298 K up to 373 K. The quoted uncertainties are the expanded uncertainties U with $U(\alpha) = 2 \times 10^{-8}$ m^2 s^{-1} and $U(\alpha) = 1 \times 10^{-8}$ m^2 s^{-1} for $LiCoO_2$ and $LiMn_2O_4$ rich samples, respectively, corresponding to a 0.95 level of confidence ($k = 2$).

the $LiCoO_2$ rich cathode sample (at 298 K, $\alpha = 4.41 \times 10^{-7}$ m^2 s^{-1}) is about factor of two higher than the $LiMn_2O_4$ rich cathode sample (at 298 K, $\alpha = 2.3 \times 10^{-7}$ m^2 s^{-1}). In dependence with the temperature, the behaviour of these two samples is also different. The change in diffusivity from 298 K to 373 K for the $LiMn_2O_4$ rich cathode was found to be nearly 4%, whereas the change for the $LiCoO_2$ rich cathode sample is steeper, up to 12%.

The thermal diffusivity of the corresponding composite layer was deduced from the respective values of the diffusivity of the cathodes taking into account each constituent layer thickness, the estimated density of the blends (Table 2), thermophysical data for aluminium and carbon layers from ref. 19 and 25, and the specific heat data of the blends from our measurements (Table 3(a)). The diffusivities of the composite blends represent about 88% and 95%, respectively, of the overall diffusivity values of their cathode material. In these evaluations, the thermal contact resistance and the values for the Biot numbers were found to be low, $<10^{-6}$ m^2 K W^{-1} and 0.001, respectively. A low contact resistance was expected due to the improved particle–particle contact and adhesion of the composite material to the current collector achieved during calendaring of these samples by the manufacturer. However, accurate values of the contact resistance could not be determined in this study.

Furthermore, the behaviour of these samples was studied for a higher temperature range. The thermal diffusivity values of the cathodes decreased with increasing temperature and were found in the same range for the temperature programs, described in the thermophysical investigations section, from 298 K up to 373 K, 473 K and 573 K (data (1), (2) and (3), respectively, in Fig. 4). No weight loss occurred up to 573 K. In the case of post heat treated samples at 673 K, a weight loss of about 2% was measured for both $LiCoO_2$ and $LiMn_2O_4$ rich cathodes. These samples were extremely fragile and, without careful handling, delamination of the composite coating from the aluminium foil could have been easily induced. Since all the constituents of the composite sample are stable up to this temperature, this could only be attributed to the decomposition of the polyvinylidene fluoride binder which occurs above 573 K[7] by a chain stripping mechanism.[7,26] Thus, due to the instability of the binder polymer, the composition of these annealed blended samples differs from the initial composition, followed by delamination of the composite layer from the current collector layer. This is observed after the heat treatment at 673 K was performed, when the measured diffusivity values were found to be lower over the whole temperature range (Fig. 4, data (4)). All the samples were carefully analysed by SEM after each heat treatment. Particularities were detected on the top of the $LiCoO_2$ rich composite after the heat treatment at 673 K (Fig. 5). The surface of the sample was found to be inhomogeneous, containing isolated molten areas which we attribute to melting of the binder. Such behaviour was not observed on the surface of the $LiMn_2O_4$ rich cathode. This could be explained by the composite matrix effect in the $LiMn_2O_4$ rich cathode, due to the lower porosity and diverse particle size (primary particles with a size below 1 μm among large particles up to 23 μm). In addition, the PVDF binder volume fraction in each sample was deduced from the weight of the sample and its composition (Table 1). Thus, in the porous $LiCoO_2$ rich composite, the binder has a higher (about 50%) volume fraction than in the porous $LiMn_2O_4$ rich composite, which leads to a different

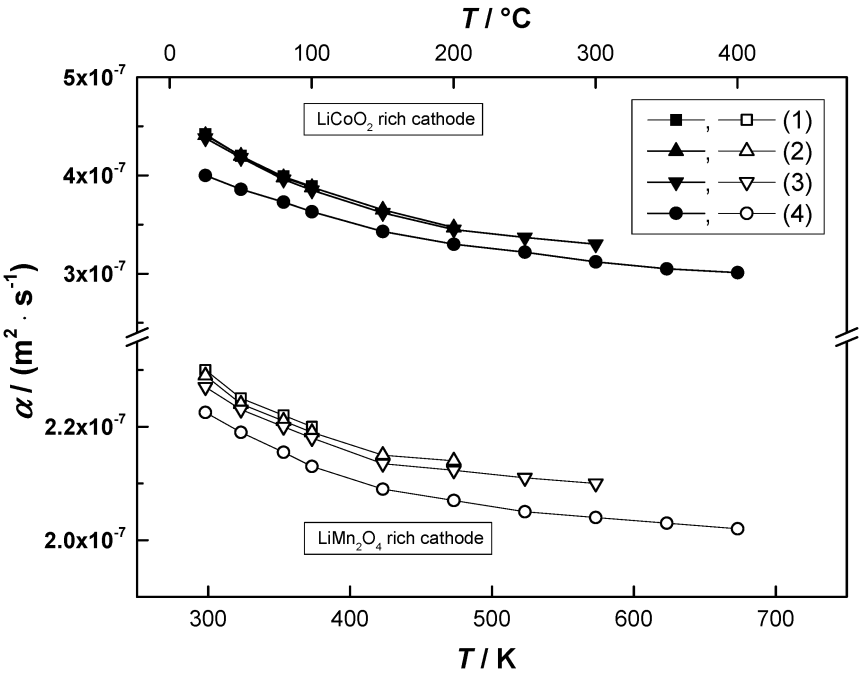

Fig. 4 The thermal diffusivity of the $LiCoO_2$–$LiMn_2O_4$ blended cathodes as a function of temperature, for the measurements performed with individual temperature programs, from 298 K up to (1) 373 K, (2) 473 K, (3) 573 K and (4) 673 K, respectively. Filled symbols represent the $LiCoO_2$ rich cathode sample, whereas empty symbols represent the $LiMn_2O_4$ rich cathode sample.

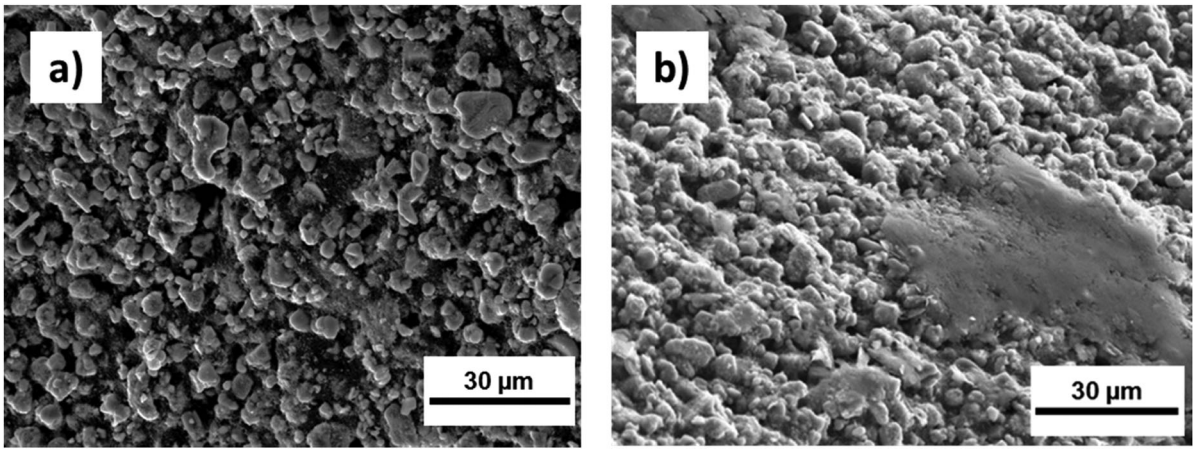

Fig. 5 SEM top view images of the $LiCoO_2$ rich cathode samples taken after performing the measurements at (a) 473 K and (b) 673 K, when inhomogeneous melting is observed on the surface of the sample.

thermal decomposition behaviour. Therefore, the thermal diffusivity of the cathode samples is governed by the composite blend morphology and the binder physical properties.

The thermal conductivity (λ) of the composite layer was calculated from the measured specific heat capacity (c_p), the thermal diffusivity (α) and the density (ρ), according to the following equation:

$$\lambda = c_p \cdot \alpha \cdot \rho. \quad (3)$$

The thermal conductivity of the $LiCoO_2$ rich composite at room temperature is λ($LiCoO_2$ rich composite) = 0.66 W m^{-1} K^{-1}, which is nearly two times higher than of the $LiMn_2O_4$ rich composite, λ($LiMn_2O_4$ rich composite) = 0.29 W m^{-1} K^{-1}. Furthermore, using relation (3), the thermal conductivity of the cathodes becomes λ($LiCoO_2$ rich cathode) = 0.79 ± 0.06 W m^{-1} K^{-1} and λ($LiMn_2O_4$ rich cathode) = 0.32 ± 0.02 W m^{-1} K^{-1}. The quoted uncertainties are the expanded uncertainties U with U(λ($LiCoO_2$ rich cathode)) = 0.06 W m^{-1} K^{-1} and U(λ($LiMn_2O_4$ rich cathode)) = 0.02 W m^{-1} K^{-1}, corresponding to a 0.95 level of confidence (k = 2). While the heat capacity and thermal diffusivity was clearly found to depend on temperature, the thermal conductivity of both samples showed no significant variation with temperature (Fig. 6). At 573 K, a decrease of about 3% from 298 K was found for the thermal conductivity of

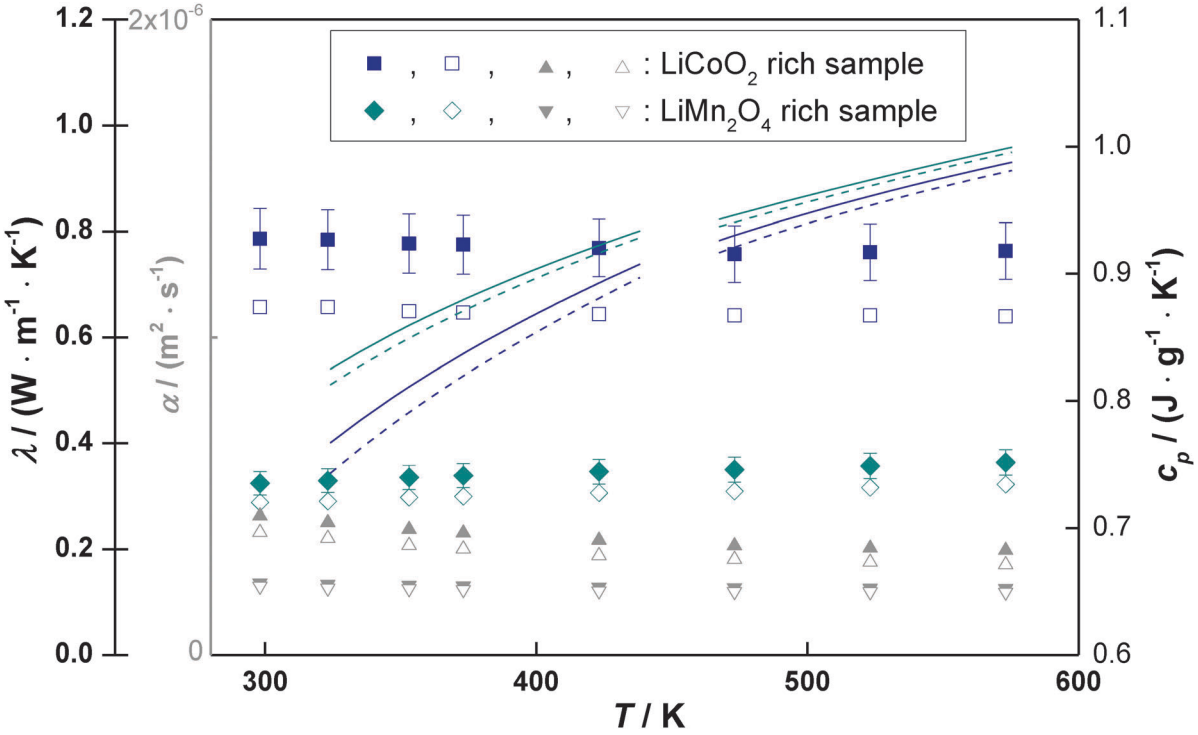

Fig. 6 Thermophysical properties in the temperature range from 298 to 573 K. Filled and empty symbols represent the cathode and composite layer values, respectively. The secondary axis shows the specific heat data of the measured composite samples (dashed lines) and the estimated cathode values (solid lines). The quoted uncertainties are the relative expanded uncertainties U_r with $U_r(\lambda) = 0.06$, corresponding to a 0.95 level of confidence ($k = 2$).

the $LiCoO_2$ rich cathode and an increase of 9% in the value for the $LiMn_2O_4$ rich cathode.

In thermal analytical models of the TMS, several assumptions are introduced to estimate the physical parameters at the interfaces between components. The thermal conductivity of the lithium-ion cell is determined from the relation between layer thicknesses and conductivities,[27] for which the effect of contact resistance at porous–porous and porous–solid interfaces is considered negligible.

Accordingly, the thermal conductivities of the cathodes can be estimated based on the combination of thickness l_i and conductivity λ_i of the constituent layer components, i:

$$\lambda(\text{cathode}) = \sum l_i / \sum (l_i/\lambda_i). \quad (4)$$

This assumption is accepted when the contact interfaces are wetted with electrolyte and all pores in the composite electrodes are filled. The obtained results for our dry samples are $\lambda(LiCoO_2$ rich cathode) = 0.80 W m^{-1} K^{-1} and $\lambda(LiMn_2O_4$ rich cathode) = 0.32 W m^{-1} K^{-1}. These values agree very well with our estimated data using eqn (3), in which the derived thermal conductivities correspond to samples with a low thermal contact resistance.

Nevertheless, in the assessment of the thermophysical properties of lithium-ion cell electrodes, aspects regarding inhomogeneity at composite level should be taken into account. Nonuniform composite morphology and porosity distribution, low particle–particle contact, poor composite layer adhesion to the current collector, dry areas existent after incomplete electrolyte wetting of the electrodes could be responsible for thermal gradients during cell operation[5] and have to be considered for a realistic description of the thermal runaway scenario.

Comparison to the available literature

The few available data on cathode material properties are collected in Table 4. None of these, however, are attributed to higher temperatures at which thermal runaway occurs,[28] *i.e.* an onset temperature above 423 K. Most electrode properties refer to the composite contribution including the electrolyte solution (wet composite),[29–32] and/or the current collector.[33–35] All these above data are difficult to compare directly due to the lack of information on active material concentration, type and amount of additives in the composite, porosity, type and amount of liquid electrolyte estimated to fill the pores, and individual layer thicknesses. Williford *et al.*[29] referred to the effective material properties in a lithium-ion battery as delivered by its manufacturer. Chen *et al.*[31] reported experimental values on a wet $LiCoO_2$ composite, yet an explicit description of the associated measurements was not provided. Fuller *et al.*[34] estimated for the first time the specific heat of $LiMn_2O_4$ cathodes, however (as in ref. 29 and 31), also without a reference for the current collector thickness. In most of these studies, for comparison we estimated the thermal diffusivity by calculations using relation (3).

Since Chen and Evans[32] reported the porosity of the positive electrode, using the electrolyte properties from ref. 36 and 37,

Table 4 Thermophysical properties of (a) $LiCoO_2$ and (b) $LiMn_2O_4$ cathode materials: available literature data and results from this study. Thickness of the material, when reported, is also included. In all the references, aluminium describes the current collector

Material/method	Specific heat ($J\ g^{-1}\ K^{-1}$)	Thermal diffusivity $\times 10^6$ ($m^2\ s^{-1}$)	Density $\times 10^{-6}$ ($g\ m^{-3}$)	Thermal conductivity ($W\ m^{-1}\ K^{-1}$)	Thickness $\times 10^6$ (m)	Ref.
(a)						
Cathode (wet)/manufacturer	1.1738	0.6021[a]	2.6175	1.85	109.224	29
Cathode (wet)/estimated	0.849	0.541[a]	2.81	1.29	—	30
Cathode (wet)/measured	1.2692	0.5346[a]	2.3285	1.58	—	31
Cathode (probably dry)/measured	0.601	1.24	3.115	2.33	185	33
Composite (wet)/estimated	1.134	0.658[a]	2.92	2.18	190	32
$LiCoO_2$ thin film/measured	0.73	—	—	5.4	0.5	38
$LiCoO_2$ in composite/estimated	0.7	0.846[a]	2.5	1.48	92	37
Electrolyte ($LiPF_6$/EC + DMC + DEC)/—	*0.1339*	2.6	1.29	0.45	—	37
Aluminium/measured	0.897	97.2	2.7	237	—	19 and 25
Cathode (dry)/measured	0.77 ± 0.02	0.44 ± 0.02	2.34 ± 0.03	0.79 ± 0.06[a]	110	This study
Composite (dry)/estimated	0.74 ± 0.02	0.39 ± 0.02	2.29 ± 0.02	0.66 ± 0.05[a]	95	This study
(b)						
Cathode (probably dry) + Al/estimated	0.713	4.108[a]	2.81	8.23	200	34 and 35
Composite (probably dry)/estimated	0.7	1.2[a]	2.5	2.1	80	46 and 47
Composite (dry)/estimated	0.7	4.8[a]	1.5	5	190	40–45
Composite (probably dry)/estimated	1.321	0.473[a]	2.37	1.48	180	48
Composite (probably dry)/estimated	1.043	1.034[a]	2.317	2.5	183	49
$LiMn_2O_4$ pellet/measured	—	94	—	—	—	39
Cathode (dry)/measured	0.83 ± 0.02	0.23 ± 0.01	1.73 ± 0.02	0.32 ± 0.02[a]	160	This study
Composite (dry)/estimated	0.81 ± 0.02	0.22 ± 0.02	1.63 ± 0.02	0.29 ± 0.02[a]	145	This study

"—": stands for "not specified".[a] Calculated using relation (3), with $\alpha(T) = \lambda(T)/(c_p(T)\cdot\rho(T))$, where $\lambda(T)$, $c_p(T)$ and $\rho(T)$ were taken from the respective reference data.

the assessed specific heat capacity of the dry $LiCoO_2$ composite in the electrode at 298 K is c_p = 1.3 J g^{-1} K^{-1}. This value is almost equal to that of the PVDF binder as obtained by Lee *et al.*[24] (Fig. 2). Generally, the specific heat of the composite is governed by the contribution of the active material for which the specific heat is lower, $c_p(LiCoO_2)$ = 0.7 J g^{-1} K^{-1},[6] and therefore the estimated composite c_p = 1.3 J g^{-1} K^{-1} is not supported here. Maleki *et al.*[33] measured the thermal properties of the electrodes in stacked layers of a commercial Sony US-18650 lithium-ion cell containing $LiCoO_2$ cathode as a function of the open circuit voltage. Based on the given physical parameters of the battery components, the estimated dry specific heat of the $LiCoO_2$ composite yields c_p = 0.57 J g^{-1} K^{-1}, which is slightly underestimated since the specific heat capacities values of the active material and additives are all above 0.6 J g^{-1} K^{-1} at 298 K. Furthermore, Bandhauer *et al.*[27] pointed out a few inconsistencies with the data from ref. 33, which refer to the thermal conductivity of the individual electrodes and the stacks. Recently, thermal conductivity of thin film $LiCoO_2$ was measured by Cho *et al.*[38] as a function of Li content, during electrochemical cycling against lithium as counter and quasi-reference electrodes. Thermal conductivity was found to decrease with delithiation, an opposite behaviour to that observed by Maleki *et al.*[33]

The available data on $LiMn_2O_4$ composites show also inconsistencies with respect to the specific heat capacity which is reported in a similar range as for the $LiCoO_2$ composite, from 0.7 to 1.3 J g^{-1} K^{-1}. A particular study was performed by Lee *et al.*,[39] in which the thermal diffusivity was studied with dependence of Li content and a comparative very low value was related to the $Li_1Mn_2O_4$ sample, $\alpha = 94 \times 10^{-6}$ m^2 s^{-1}.

Generally, the thermal conductivity data seem to be overestimated in all references. In the case of the $LiMn_2O_4$ cathode, density and specific heat values from ref. 40–45 and 40–47, respectively, are close to our data. The composite data adopted by Cheng *et al.*[48] and Wu *et al.*[49] are overrated. However, the thermal conductivity data given in these literatures seem to be too high, even in comparison to the other reference data, which obviously lead to increased values of resulted thermal diffusivities. Consequently, using relation (3), the thermophysical data for aluminium[19,25] and electrolyte,[37] the obtained thermal diffusivity in the wet composites and cathodes from ref. 29–32, are within the same range as our results. Additionally, we need to consider the composition of our cathode samples. The $LiCoO_2$ rich cathode contains a blend of $LiCoO_2$ with $LiMn_2O_4$ active material in a molar ratio of 3.9 : 1.0. In the $LiMn_2O_4$ rich cathode, the active material is mainly $LiMn_2O_4$ ($LiMn_2O_4$: $LiCoO_2$ = 29.7 : 1.0). Therefore, based on the measured thermal diffusivity of the $LiMn_2O_4$ rich cathode, which was found to be lower than the value of $LiCoO_2$ rich cathode, we assume a higher thermal conductivity for a cathode containing pure $LiCoO_2$ active material, which concludes in a better agreement with the estimated literature data.

Conclusions

Two commercial cathode materials relevant for lithium-ion batteries were studied in this work and their thermophysical properties were evaluated as function of temperature up to 673 K. These samples are based on aluminium foil (substrate, current collector) coated on a single side by a composite layer

which is a mixture of active materials and additives. The active materials were blends of $LiCoO_2$ and $LiMn_2O_4$ with the molar ratio 3.9 : 1.0 ($LiCoO_2$ rich cathode) and 29.7 : 1.0 ($LiMn_2O_4$ rich cathode), and 0.940 total mass fraction of in powder.

The specific heat capacities were determined from the measured composite heat capacity using two differential scanning calorimeters and the contribution of the aluminium substrate in relation to their mass fraction. Thermal diffusivities were measured by laser flash technique and the composite thermal conductivity was evaluated based on the layers model. Thermal conductivity data were calculated using the specific heat capacities, the thermal diffusivities and the estimated densities. While the specific heat capacity of $LiMn_2O_4$ rich sample is slightly higher than that of the $LiCoO_2$ rich sample, the thermal diffusivity and density are lower. Taking into account also the differences in morphology and porosity, the thermal conductivity of $LiCoO_2$ cathodes are factor of two lower than $LiMn_2O_4$. It has been found that the measured specific heat capacity and the thermal diffusivity of both cathodes blends increase with temperature. In both samples, the thermal conductivity behaviour with temperature is nearly constant.

In this study, the measured thermophysical properties and their reported temperature dependency are the first reports of this kind. Such data are valuable for the simulation models of thermal behaviour, including thermal runaway describing a high temperature scenario and for which, up to now, the input parameters are assumed temperature independent.

Acknowledgements

The authors thank M. Rohde and D. M. Cupid (KIT, IAM – AWP) for the discussions related to the thermophysical properties. Furthermore we acknowledge the highly appreciated contribution of the following persons: T. Bergfeldt and A. Reif (KIT, IAM – AWP) for the ICP-OES and WDXRF analyses, and SEM and LM measurements, respectively, M. Schwotzer and T. Sollich (KIT, IFG) for the mercury porosimetry analysis, T. Markus and M. Ziegner (FZ Jülich) for the XRD and Rietveld analysis. The authors are grateful to W. Pfleging (KIT, IAM-AWP) and the support from the Karlsruhe Nano Micro Facility (KNMF, http://www.knmf.kit.edu/) for laser cutting of the electrodes. Financial support from the Helmholtz Association of German Research Centres through the Portfolio topic ''In-system Electrochemical Storage – Reliability and Integration'' is gratefully acknowledged.

References

1 S. B. Chikkannanavar, D. M. Bernardi and L. Liu, *J. Power Sources*, 2014, **248**, 91.
2 Ya. V. Shatilo, E. V. Makhonina, V. S. Pervov, V. S. Dubasova, A. F. Nikolenko, Zh. V. Dobrokhotova and I. A. Kedrinskii, *Inorg. Mater.*, 2006, **42**(7), 782.
3 N. V. Kosova, E. T. Devyatkina and V. V. Kaichev, *Russ. J. Electrochem.*, 2009, **45**(3), 277.
4 A. Manthiram and T. Muraliganth, in *Handbook of Battery Materials*, ed. C. Daniel and J. O. Besenhard, Wiley-VCH Verlag & Co. KGaA, Germany, 2011, p. 343.
5 M. Wu, T. Liao, Y. Wang and C. Wan, *J. Appl. Electrochem.*, 2004, **34**, 797.
6 P. Gotcu-Freis, D. M. Cupid, M. Rohde and H. J. Seifert, *J. Chem. Thermodyn.*, 2015, **84**, 118.
7 http://www.mtixtl.com.
8 http://www.linseis.com.
9 M. R. Kronthaler, F. Schloegl, J. Kurfer, R. Wiedenmann, M. F. Zaeh and G. Reinhart, *Phys. Procedia*, 2012, **39**, 213.
10 J. S. Kim, R. Kohler, W. Pfleging, H. J. Seifert, D. Byun, H.-G. Jung and J.-K. Lee, *J. Power Sources*, 2015, **279**, 13.
11 W. J. Parker, R. J. Jenkins, C. P. Butler and G. L. Abbott, *J. Appl. Phys.*, 1961, **32**(9), 1679.
12 L. Dusza, *High Temp. - High Pressures*, 1995, **27/28**, 467.
13 L. Dusza, *High Temp. - High Pressures*, 1996, **27/28**, 475.
14 H. J. Lee, *Thermal Diffusivity in Layered and Dispersed Composites*, PhD thesis, Purdue University, Lafayette, IN, USA, 1975.
15 K. Mizushima, P. C. Jones, P. J. Wiseman and J. B. Goodenough, *Mater. Res. Bull.*, 1980, **15**, 783.
16 E. Antolini, *Solid State Ionics*, 2004, **170**, 159.
17 Y. Gao and J. R. Dahn, *J. Electrochem. Soc.*, 1996, **143**(6), 1783.
18 M. Wang and A. Navrotsky, *J. Solid State Chem.*, 2005, **178**, 1182.
19 *Thermophysical Properties of Matter: CD-ROM Set*, ed. Y. S. Touloukian, Purdue Research Foundation, 2003.
20 H. Zheng, L. Tan, G. Liu, X. Song and V. S. Battaglia, *J. Power Sources*, 2012, **208**, 52.
21 M. Yoshio and H. Noguchi, A review of positive electrode materials for lithium-ion batteries, in *Lithium-Ion Batteries*, ed. M. Yoshio, R. J. Brodd and A. Kozawa, Springer, 2009.
22 A. V. Knyazev, M. Maczka, N. N. Smirnovy, S. S. Knyazeva, N. G. Chernorukov, M. Ptak and A. N Shushunov, *Thermochim. Acta*, 2014, **593**, 58.
23 G. Rousse, C. Masquelier, J. Rodriguez-Carvajal, E. Elkaim, J.-P. Lauriat and J. L. Martinez, *Chem. Mater.*, 1999, **11**, 3629.
24 W. K. Lee and C. L. Choy, *J. Polym. Sci.*, 1975, **13**, 619.
25 M. W. Chase, *NIST-JANAF Themochemical Tables*, Fourth Edition, *J. Phys. Chem. Ref. Data*, 1998, Monograph 9, 1.
26 Thermal decomposition of polymers, in *SFPE Handbook of Fire Protection Engineering*, ed. C. L. Beyler and M. H. Hirschler, National Fire Protection Association, 2002, ch. 7.
27 T. M. Bandhauer, S. Garimella and T. F. Fuller, *J. Electrochem. Soc.*, 2011, **158**(3), R1–R25.
28 A. W. Golubkov, D. Fuchs, J. Wagner, H. Wiltsche, C. Stangl, G. Fauler, A. Thaler and V. Hacker, *RSC Adv.*, 2014, **4**, 3633.
29 R. E. Williford, V. V. Viswanathan and J.-G. Zhang, *J. Power Sources*, 2009, **189**, 101.
30 K. Kanari, K. Takano and Y. Saito, *Bull. Electrochem. Lab*, 1996, **60**, 65, Umezono, Ibaraki, 305 Japan.
31 S. C. Chen, C. C. Wan and Y. Y. Wang, *J. Power Sources*, 2005, **140**, 111.
32 Y. Chen and J. W. Evans, *J. Electrochem. Soc.*, 1996, **143**(9), 2708.
33 H. Maleki, S. A. Hallaj, J. R. Selman, R. B. Dinwiddie and H. Wang, *J. Electrochem. Soc.*, 1999, **146**(3), 947.

34 T. F. Fuller, M. Doyle and J. Newman, *J. Electrochem. Soc.*, 1994, **141**(1), 1.
35 J. Newman and W. Tiedemann, *J. Electrochem. Soc.*, 1995, **142**(4), 1054.
36 G. Guo, B. Long, B. Cheng, S. Zhou, P. Xu and B. Cao, *J. Power Sources*, 2010, **195**, 2393.
37 P. Peng, Y. Sun and F. Jiang, *Heat Mass Transfer*, 2014, **50**, 1405.
38 J. Cho, M. D. Losego, H. G. Zhang, H. Kim, J. Yuo, I. Petrov, D. G. Cahill and P. V. Braun, *Nat. Commun.*, 2014, **5**, 4035.
39 S. T. Lee, K. Raveendranath, M. R. Tomy, M. Paulraj, S. Jayalekshmi, K. P. R. Nair and J. Ravi, *Phys. Rev. B: Condens. Matter Mater. Phys.*, 2007, **76**, 115112.
40 M. Doyle, J. Newman, A. S. Gozdz, C. N. Schmutz and J.-M. Tarascon, *J. Electrochem. Soc.*, 1996, **143**(6), 1890.
41 *Lithium Batteries*, ed. S. Surampudi, R. A. Marsh, Z. Ogumi and J. Prakash, The Electrochemical Society Proceedings Series, Pennington, NJ, 2000.
42 V. Srinivasan and C. Y. Wang, *J. Electrochem. Soc.*, 2003, **150**(1), A98–A106.
43 K. Smith and C. Y. Wang, *J. Power Sources*, 2006, **161**, 628.
44 U. S. Kim, J. Yi, C. B. Shin, T. Han and S. Park, *J. Power Sources*, 2011, **196**, 5115.
45 S. Mazumder and J. Lu, *Int. J. Electrochem.*, 2013, 268747.
46 K. Kumaresan, G. Sikha and R. E. White, *J. Electrochem. Soc.*, 2008, **155**(2), A164–A171.
47 P. W. C. Northrop, V. Ramadesigan, S. De and V. R. Subramanian, *J. Electrochem. Soc.*, 2011, **158**(12), A1461–A1477.
48 L. Cheng, C. Ke, S. Fengshun, T. Peng and Z. Hongwei, *Vehical and Propulsion Power Conference*, IEEE Publisher, 2009, p. 1643, ISBN 978-1-4244-2600-3.
49 W. Wu, X. Xiao and X. Huang, *Proceedings of the ASME 2011 5th International Conference on Energy Sustainability*, Washington, DC, USA.